Proc. of the 8th International Symposium on Geotechnical Safety and Risk (ISGSR)
Edited by Jinsong Huang, D.V. Griffiths, Shui-Hua Jiang, Anna Giacomini and Richard Kelly
 Published by Research Publishing, Singapore.
doi: 10.3850/978-981-18-5182-7_21-007-cd

ISGSR 2022

Towards Stochastic Structural and Geotechnical Design for Solar Array Foundation Design

Richard Kelly[1], Yuting Zhang[2], Jinsong Huang[3], Scott Chamberlain[4]

[1]SMEC, Level 6 480 St Pauls Terrace, Brisbane.
E-mail: drrichard.kelly@smec.com
[2]Discipline of Civil, Surveying and Environmental Engineering, The University of Newcastle, Callaghan, NSW 2308, Australia
E-mail: yuting.zhang11@uon.edu.au
[3]Discipline of Civil, Surveying and Environmental Engineering, The University of Newcastle, Callaghan, NSW 2308, Australia
E-mail: jinsong.huang@newcastle.edu.au
[4]SMEC, Level 6 480 St Pauls Terrace, Brisbane.
E-mail: scott.chamberlain@smec.com

Abstract: Use of reliability analyses to assess the probability of failure for solar farm foundations has the potential to provide significant capital cost savings to an asset owner if consequent increases in maintenance cost are manageable. Reliability analyses are described and some initial thoughts about assessing soil properties as a function of wind and rain are discussed.

Keywords: LRFD; Solar farms; foundations; correlated wind and rain.

1 Introduction

Power consumption in Australia is projected to nearly double from 180TWh to 320TWh by 2050 (AEMO ISP, 2022; CEC Clean Energy Report, 2022). In the past 5 years, 9.8 GW of renewables have been constructed. Australia needs to build 28 GW of wind and solar by 2030, reaching 81 GW by 2040 then 140 GW by 2050. Utility Solar is likely to comprise around 30% of generation capacity (i.e., 70 GW over this time). Utility solar arrays are usually supported by piles and there is typically about 1 pile per 2kW of energy. Therefore about 35 million piles will need to be constructed between now and 2050. A typical 3.6 m long galvanized steel H pile costs about $86AUD each to procure. The total cost of materials for piles will be in the order of $3 billion dollars. If the piles could be made lighter, shorter and ungalvanized, their material cost could reduce by at least $30 per pile resulting in a capital cost saving in the order of $1 billion dollars.

Use of conventional Australian Standards results in foundations for solar arrays being designed using sacrificial steel and galvanising to withstand the ultimate wind loading event on the last day of operation. That means the asset owner pays for extra steel and galvanising to achieve a very small probability of failure. An alternative approach is to reduce the thickness of steel, reduce the post length and try and eliminate galvanising. These reductions will increase the probability of failure and hence increase maintenance at the same time as reducing capital cost. Providing the reduction in capital cost sufficiently outweighs the increase in maintenance and associated risk then there is benefit to the asset owner.

Australian Standard AS5104 Structural Reliability can be used to develop the alternative approach while also conforming to the National Construction Code.

Here, we briefly outline what is required to perform these analyses and present some initial thoughts about estimating the depth of wetting front of the ground. First, the Maximum Likelihood Estimation (MLE) method is used to prove the existing data set covers the required 100-year return period wind speed. Then, the resampling method is used to sample wind and rainfall data directly. Finally, the Green–Ampt Mein-Larson (GAML) model is adopted to derive the distribution of the depth of wetting front.

2 Structural Reliability Analyses

A structural reliability analysis is a stochastic analysis that requires inputs as probability density functions (PDF) and performs Monte-Carlo calculations to estimate probabilities of structural or geotechnical failure. Inputs to such analyses are:

1. Wind speed, wind direction, rainfall and evaporation data from the Bureau of Meteorology and on site weather stations
2. PDFs for wind pressure coefficients acting on solar arrays
3. PDFs for structural and geotechnical material parameters and geometries

4. PDFs for rates of corrosion of steel and potentially galvanised steel
5. The analyses require:
    a. Correlations between antecedent rainfall over periods of time, wind speed, wind direction and evaporation
    b. Top of pile loads
    c. Monte Carlo analyses incorporating
        i. An ability to compute the structural capacity of a pile each year over the design life factoring in effects of corrosion on effective thickness of (galvanised) steel
        ii. Computing the strength of the ground as a function of rainfall and evaporation
        iii. An ability to compute the lateral geotechnical capacity of a pile
    d. Allow for the spatial correlation of pile performance based on correlated wind speeds, geotechnical conditions and corrosion
6. Economic assessment to calculate the reduction in capital cost, potential reduction in borrowing cost and potential increase in maintenance cost, along with any other factors not considered
7. Understanding and written acceptance by the asset owner and any other stakeholders, such as insurers and bankers, of the proposed approach and the risks and opportunities associated with this approach

The structural capacity of solar array foundations is controlled by lateral-torsional buckling which in turn is a function of the cantilever length of the array post. Piles can buckle at the ground surface if the ground has sufficient strength but may buckle below the ground surface if the ground is weak (Lee et al., 2019). The strength of the ground is a function of its moisture content with depth. The depth of wetting is a function of the period of time rainfall occurs. The probability of structural failure will increase if the ground is weak at the same time the design wind event occurs. The probability that the ground is wet at the same time as the design wind event occurs is required for a reliability analysis to be performed. Bureau of Meteorology data is assessed to correlate various periods of rainfall with wind speed in order to develop a joint probability distribution function from which extreme values can be extracted. The probability of structural failure also increases as corrosion increases over time. However, ground conditions are independent of corrosion and do not necessarily need to be treated in a time dependent calculation.

3 Correlation between wind and rain

Maximum wind speed and daily rainfall data were obtained from the Bureau of Meteorology for the Nobbys Beach site in Newcastle between 01/01/1969 to 14/07/2022. Comparisons between daily wind speeds and different periods of antecedent rainfall are provided in Figures 1 to 4. There is essentially no correlation between antecedent rainfall and maximum daily wind speed. The data can also be expressed as joint probability histograms. Examples for 7 day and 30 day antecedent rainfall are presented in Figures 5 and 6.

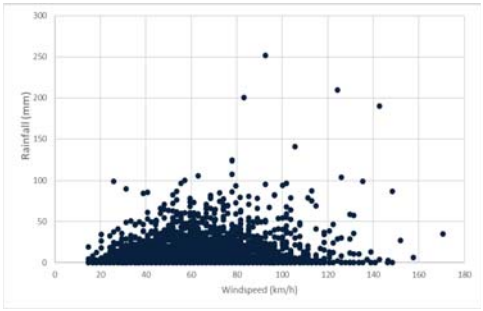

Figure 1. Wind speed and daily rainfall.

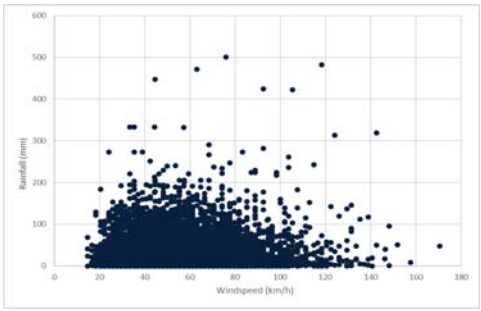

Figure 2. Wind speed and 7 day antecedent rainfall.

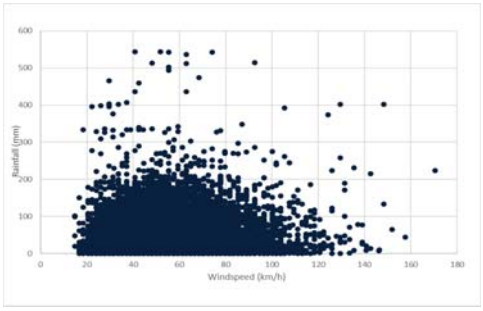

Figure 3. Wind speed and 14 day antecedent rainfall.

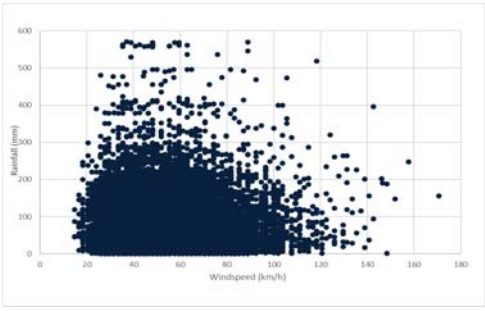

Figure 4. Wind speed and 30 day antecedent rainfall.

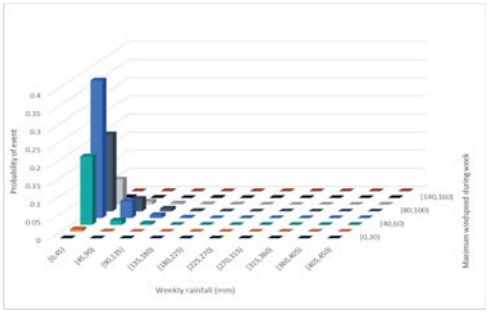

Figure 5. Joint probability of wind speed and 7 day antecedent rain.

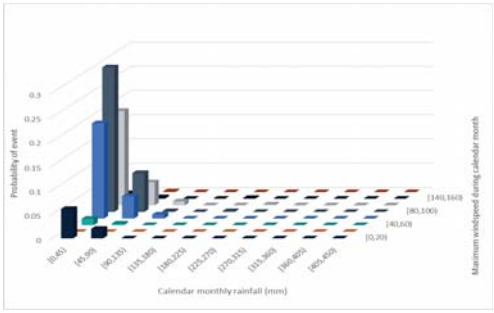

Figure 6. Joint probability of wind speed and 30 day antecedent rain.

4 Approaches to sample wind and rainfall

Two approaches can be used to sample wind and rainfall. Approach A: Resampling historical rainfall and wind records; Approach B: Sampling probability distribution of rainfall and wind. Below, a brief introduction to these two approaches is given.

4.1 Resampling historical rainfall and wind records

Approach A directly sample the wind and rainfall data from the data set. Randomly sample a date to obtain the wind speed and different periods of antecedent rainfall. Repeat the process 365*100 times, as the design wind speed is for the 100-year return period. This method can directly handle correlations between wind and rainfall. Besides, the rainfall pattern is also reflected in the real rainfall data if high resolution records are available, e.g., rainfall data is recorded every minute. The problem with this approach is that the fact that the wind record is long enough to cover the 100-year return period wind speed needs to be proven first. In this paper, the Maximum Likelihood Estimation (MLE) method is adopted.

The MLE method consists of finding the value of the parameter vector that maximizes the likelihood function and therefore makes the observed data most likely (Naghettini, 2017). Let $x=\left(x_1,x_2,...,x_n\right)$ represent a set of n independent and identically distributed observed data and $f\left(x,\theta\right)$ is the probability distribution function with parameter θ. The likelihood function L can be written as follows:

$$L=\prod_{i=1}^{n} f_X\left(x_i\right) \tag{1}$$

In this case $\hat{\theta}$ is said to be the MLE of θ if $\hat{\theta}$ maximizes the likelihood function L. In this paper, the maximum wind speed is assumed to follow the generalized extreme value (GEV) distribution (Jenkinson, 1955). The parameters of the GEV distribution are derived based on the MLE method, and the obtained distribution is further used to calculate the corresponding return period for the observed data. Figure 7 shows that the maximum of the recorded maximum wind speed corresponds to 173 years return period, which means approach A is feasible for the Nobbys Beach site. Therefore, approach A is adopted to sample wind and 7 days antecedent rainfall data, which are further used as inputs to generate the depth of wetting front.

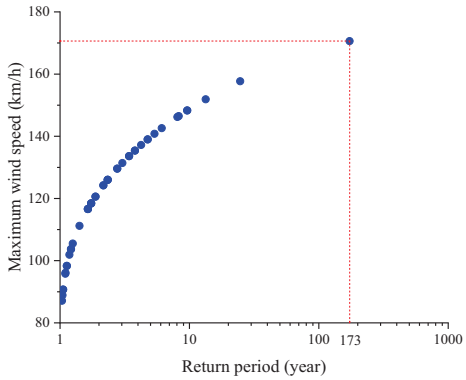

Figure 7. Relationship between maximum wind speed and return period.

4.2 Sampling probability distribution of rainfall and wind

If the results show that 100-year return wind is not included in the data set, approach B should be used. The steps of approach B are summarized as follows:

Step 1: Investigate the correlation between rainfall and wind. The results in section 3 show that there are no clear correlations between rainfall and wind.

Step 2: Generate two marginal distributions (no correlations) based on the historical rainfall and wind data, and sample wind and rainfall separately.

Step 3: Since the depth of wetting front in the ground needs to be worked out, rainfall pattern matters. Random rainfall patterns over 7 days need to be generated as inputs to derive the depth of wetting front.

5 Depth of wetting front

5.1 Green-Ampt model

The Green–Ampt (GA) model (Green & Ampt, 1911) was originally developed to describe the infiltration in homogeneous soil under ponding conditions. The model assumes that a sharp wetting front separates the upper saturated zone and lower unsaturated zone. Based on these assumptions, the GA model is written as follows:

$$f(t) = K\left[1 + \frac{\psi\Delta\theta}{F(t)}\right] \tag{2}$$

$$F(t) = Kt + \psi\Delta\theta \ln\left[1 + \frac{F(t)}{\psi\Delta\theta}\right] \tag{3}$$

where $f(t)$ is the infiltration rate, K is the hydraulic conductivity, ψ is the suction head, $\Delta\theta$ is the increase in soil moisture during infiltration, $F(t)$ is the cumulative infiltration.

In the original form of the GA model, it is assumed that the water starts ponding on the soil surface from the beginning of the rainfall event, the curve D in Figure 8 shows this situation. However, this is usually not the case, especially during the initial period of a rainfall event when the rainfall intensity is less than the infiltration rate. Thus, Mein and Larson (1973) proposed a modified GA model, which is commonly called the Green–Ampt Mein-Larson (GAML) model. The GAML model divides the infiltration process into two stages (line B and curve C in Figure 8). In the first stage (line B), all the rainfall infiltrates into the soil, and the depth of the wetting front gradually increases. In the second stage (curve C), the surface is ponded at t_p and the infiltration rate gradually decreases. The equations calculate the cumulative infiltration of the GAML model as follows:

$$\begin{aligned} F(t) &= it && \text{for } t \le t_p \\ F(t) &= K\left(t - t_p\right) + \psi\Delta\theta \ln\left[\frac{\psi\Delta\theta + F(t)}{\psi\Delta\theta + F_p}\right] && \text{for } t > t_p \end{aligned} \tag{4}$$

where i is the rainfall intensity, t_p is the ponding time, F_p is the cumulative infiltration at ponding time.

At the ponding time t_p, the infiltration rate is equal to the rainfall intensity. Therefore, substituting $f(t) = i$ and $F(t) = it_p$ into Eq. (2) results in the ponding time as follows:

$$t_p = \frac{K\psi\Delta\theta}{i(i-K)} \tag{5}$$

For line A in Figure 8, the ponding condition will never occur as all the rainfall infiltrates. In this case, the cumulative infiltration equals the cumulative rainfall.

Based on the cumulative infiltration, the depth of wetting front L_d is determined as follows:

$$L_d = \frac{F(t)}{\Delta\theta} \tag{6}$$

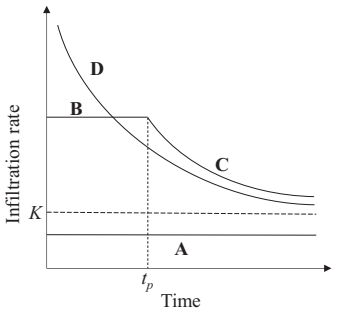

Figure 8. Different cases of infiltration behaviour under rainfall (Mein & Larson, 1973).

5.2 Example

Application of the GAML model requires the determination of two key parameters, the suction head ψ and the hydraulic conductivity K (Ma et al., 2010), which are inherent to the soil, the soil cover and the initial soil moisture (Van Mullem, 1989). Several methods have been proposed to determine the ψ from measured soil hydraulic properties (Bouwer, 1969; Neuman, 1976). Brakensiek and Onstad (1977) indicated that the infiltration and runoff quantities are more sensitive to K with respect to ψ, and extensive studies have been carried out to derive the value of K (Risse et al., 1994; Van den Putte et al., 2013). In this paper, the parameters used in the GAML model are summarized in Table 1. For the purpose of demonstration, the constant rainfall intensity is assumed, and the duration of rainfall event is calculated as rainfall/rainfall intensity. To consider the rainfall patterns in approach A, minutes or hours based rainfall data sets are required. The duration of a rainfall event is divided into many short periods, so that the rainfall intensity is essentially constant within each period.

Table 1. Summary of parameters used in the GAML model

Parameter	K, cm/h	ψ, cm	$\Delta\theta$	i, cm/h
Value	2.3	29.22	0.23	0.2, 1.5, 2.3, 5, 10, 20

5.3 Results

Figures 9 and 10 show the distribution and corresponding statistics of the depth of wetting front under various rainfall intensities. When the rainfall intensity is less than the hydraulic conductivity, the influence of rainfall intensity on the depth of wetting front is negligible since all the rainfall infiltrates into the soil. In contrast, when the rainfall intensity is larger than the hydraulic conductivity, the maximum and mean depth of wetting front significantly decrease as the rainfall intensity increases. The reason is that, for the same cumulative rainfall, the duration of a rainfall event is inversely proportional to rainfall intensity, and less rainfall infiltrates into the soil under larger rainfall intensity.

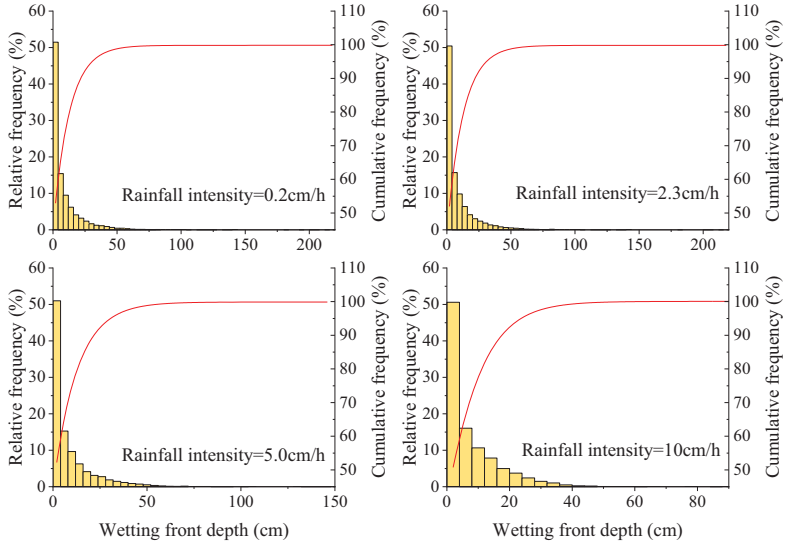

Figure 9. Distribution of the depth of wetting front under various rainfall intensities.

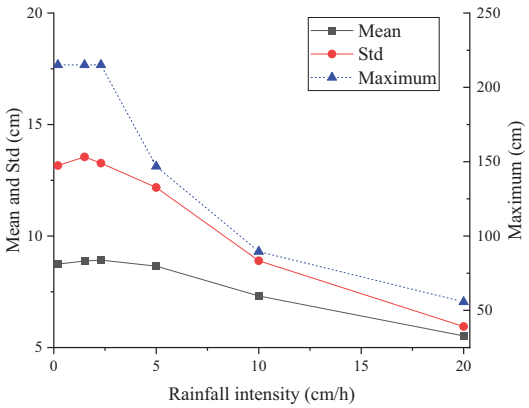

Figure 10. Statistics of the depth of wetting front under various rainfall intensities.

6 Concluding remarks

This paper presents an initial thought on estimating the depth of wetting front with the wind and rainfall data set. The resampling method is proven to be feasible for the Nobbys Beach site. The distribution of the depth of wetting front is sensitive to the rainfall intensity when the rainfall intensity exceeds the hydraulic conductivity. The proposed process will be further used to perform reliability analyses of solar farm foundations under wind and rainfall conditions.

References

Australian Energy Market Operator (AEMO), (2022). Integrated System Plan for the National Electricity market, https://aemo.com.au/-/media/files/major-publications/isp/2022/2022-documents/2022-integrated-system-plan-isp.pdf?la=en

Bouwer, H. (1969). Infiltration of water into nonuniform soil. *Journal of the Irrigation and Drainage Division*, *95*(4), 451-462.

Brakensiek, D. L., & Onstad, C. A. (1977). Parameter estimation of the Green and Ampt Infiltration Equation. *Water Resources Research*, *13*(6), 1009-1012.

Clean Energy Council (CEC), (2022). Clean Energy Australia Report, https://www.cleanenergycouncil.org.au/resources/resources-hub/clean-energy-australia-report

Green, W. H., & Ampt, G. A. (1911). Studies on Soil Phyics. *The Journal of Agricultural Science*, *4*(1), 1-24.

Jenkinson, A. F. (1955). The frequency distribution of the annual maximum (or minimum) values of meteorological elements. *Quarterly Journal of the Royal Meteorological Society*, *81*(348), 158-171.

Lee, C., Ng, C., & Kelly, R. (2019). *Predicting in-ground buckling instability of the steel H-beam pile through nonlinear analysis* Proc. 13th Australia New Zealand Conference on Geomechanics, Sydney, Australia.

Ma, Y., Feng, S., Su, D., Gao, G., & Huo, Z. (2010). Modeling water infiltration in a large layered soil column with a modified Green–Ampt model and HYDRUS-1D. *Computers and Electronics in Agriculture*, *71*, S40-S47.

Mein, R. G., & Larson, C. L. (1973). Modeling infiltration during a steady rain. *Water Resources Research*, *9*(2), 384-394.

Naghettini, M. (2017). *Fundamentals of statistical hydrology*. Springer.

Neuman, S. P. (1976). Wetting front pressure head in the infiltration model of Green and Ampt. *Water Resources Research*, *12*(3), 564-566.

Risse, L. M., Nearing, M. A., & Savabi, M. R. (1994). Determining the Green-Ampt effective hydraulic conductivity from rainfall-runoff data for the WEPP model. *Transactions of the ASAE*, *37*(2), 411-418.

Van den Putte, A., Govers, G., Leys, A., Langhans, C., Clymans, W., & Diels, J. (2013). Estimating the parameters of the Green–Ampt infiltration equation from rainfall simulation data: Why simpler is better. *Journal of Hydrology*, *476*, 332-344.

Van Mullem, J. A. (1989). *Applications of the Green-Ampt infiltration model to watersheds in Montana and Wyoming*. Montana State University-Bozeman, College of Engineering.